

Article

Assessment of Manufacturing Parameters for New 3D-Printed Heating Circuits Based on CNT-Doped Nanocomposites Processed by UV-Assisted Direct Write

Alejandro Cortés , Alberto Jiménez-Suárez , Mónica Campo , Alejandro Ureña  and Silvia G. Prolongo 

Materials Science and Engineering Area, Escuela Superior de Ciencias Experimentales y Tecnología, Universidad Rey Juan Carlos, Calle Tulipán s/n, 28933 Móstoles, Spain; monica.campo@urjc.es (M.C.); alejandro.urena@urjc.es (A.U.); silvia.gonzalez@urjc.es (S.G.P.)

* Correspondence: alejandro.cortes@urjc.es (A.C.); alberto.jimenez.suarez@urjc.es (A.J.-S.); Tel.: +34-914887141 (A.C.); +34-914888252 (A.J.-S.)

Abstract: This work consists of the development of an easy strategy to transform any structure into an efficient surface heater by the application of a low voltage over 3D printed nanocomposite circuits. To this end, the electrical conductivity and self-heating capabilities of UV-Assisted Direct Write 3D printed circuits doped with carbon nanotubes were widely explored as a function of the number of printed layers. Moreover, an optimization of the printing process was carried out by comparing the accuracy and printability obtained when printing with two different configurations: extruding and curing the ink in the same stage or curing the extruded ink in a second stage, after the whole layer was deposited. In this regard, the great homogeneity and repeatability of the heating showed by the four-layer printed circuits, together with their excellent performance for long heating times, proved their applicability to convert any structure to a surface heater. Finally, the deicing capability of the four-layer circuit was demonstrated, being able to remove a 2.5 mm thick ice layer in 4 min and 4 s.

Keywords: nanocomposites; 3D printing; direct write; carbon nanotubes; self-heating; joule effect



Citation: Cortés, A.; Jiménez-Suárez, A.; Campo, M.; Ureña, A.; Prolongo, S.G. Assessment of Manufacturing Parameters for New 3D-Printed Heating Circuits Based on CNT-Doped Nanocomposites Processed by UV-Assisted Direct Write. *Appl. Sci.* **2021**, *11*, 7534. <https://doi.org/10.3390/app11167534>

Academic Editor: Anming Hu

Received: 16 July 2021

Accepted: 16 August 2021

Published: 17 August 2021

Publisher's Note: MDPI stays neutral with regard to jurisdictional claims in published maps and institutional affiliations.



Copyright: © 2021 by the authors. Licensee MDPI, Basel, Switzerland. This article is an open access article distributed under the terms and conditions of the Creative Commons Attribution (CC BY) license (<https://creativecommons.org/licenses/by/4.0/>).

1. Introduction

In recent years, 3D printing is becoming a strong alternative to traditional manufacturing techniques, especially for small production batches or fully customized parts since it reduces the initial cost due to the fact that it does not require tooling [1]. Moreover, there are other additional advantages, such as the almost total freedom regarding part geometry complexity, the ability to shorten the supply chain or the rapid prototyping capabilities, among others [2–6]. However, the lack of available 3D printing inks doped with nanofillers, which provide multifunctional capabilities, is still a significant drawback to establishing itself as a leading technology in its field [7]. Some interesting and recent examples of nanodoped inks use zeolite fillers to enhance mechanical properties and shape memory capabilities [8], boron nitride nanoparticles for enhancing thermal conductivity [9] or nano-hydroxylapatite filled polycaprolactone nanocomposites for drug-eluting purposes [10]. Nevertheless, there is still an extensive field of research regarding the development of new 3D printed polymers and nanocomposites with enhanced properties and new functionalities.

There are several 3D printing techniques that can be used depending on the material type [11]. Some examples are Fused Deposition Modelling (FDM), Stereolithography (SLA), Binder Jetting (BJ), Selective Laser Sintering (SLS) or Direct Write (DW), among others. More specifically, Direct Write technique, which consists of extruding a viscous paste through a pressurized syringe, layer by layer, until the whole three-dimensional part is completed, is an interesting 3D printing technology commonly used for high viscosity thermoset polymers or nanocomposites [12]. In addition, Direct Write technology presents

some advantages with regard to other additive manufacturing techniques, as Binder Jetting or Material Jetting, since there is no need for using neither piezoelectric nor thermal printing nozzles, which lowers the costs and maintenance [13]. Some interesting research studies, which use Direct Write technology to develop new and different multifunctional printed materials, are the one of Alexander D. Valentine et al. [14] based on hybrid 3D printing of soft electronics, the study of A Asghari Adib et al. [15] based on the development of a biomaterial for intracorporeal tissue engineering or the one of Fanli Yang et al. [16], who optimized the food printing with lemon juice gel.

Moreover, UV-Assisted Direct Write technology is an excellent alternative for printing thermoset polymers and nanocomposites since it allows for curing of each printed layer within a few seconds due to the fast photopolymerization of the extruded paste [17]. Some interesting studies of UV-Assisted Direct Write 3D printed composites are the study of Alan Shen et al. [18] based on polymer-bonded permanent magnets of arbitrary shapes, the study of Aditya Thakur et al. [19] related to printing multifunctional composites by depositing continuous carbon fiber simultaneously with functional photopolymer resin and the study of Hongqiu Wei et al. [20], based on iron oxide doped shape memory composites.

Regarding Direct Write 3D printing technology, Carbon Nanotubes (CNTs) are excellent fillers for developing smart and functional composites since they enhance printability due to the increase in the viscosity of the ink in around one order of magnitude by adding relatively low CNT contents (below 1 wt.%) and, in addition, allow for obtaining electrically conductive parts [17,21]. Moreover, the CNT addition above the electrical percolation threshold allows for exploitation of different capabilities of these nanocomposites as the strain is self-sensing [22,23] or self-heating by Joule's effect [24,25]. Some interesting studies of CNT doped UV-Assisted Direct Write printed nanocomposites are the studies of Yihui Luo et al. [26] and R Farahani et al. [27] regarding strain-monitoring sensors or the one of B Aïssa et al. [28] about carbon nanotube/polyurethane composite based field effect transistors.

Regarding the outstanding self-heating capabilities of CNT doped nanocomposites, it is possible to use them in many different applications, avoiding the need for using external heating sources as conventional ovens, blankets or complex duct systems for hot airflow [29]. Some interesting applications are self-heating foams [30] and wearable fabrics [31] that can be used for comfort purposes, or self-heating pavements with deicing capabilities [32]. Moreover, there are some other interesting studies about using CNT doped nanocomposites for anti-icing and deicing purposes in big structures with an aerodynamic profile as aircraft wings or wind turbine blades [33,34]. In this context, one of the main advantages is the relatively low power consumption, while the current deicing techniques have a power consumption up to 1 to 4% loss of annual energy production, depending on icing severity [29].

In the present paper, the self-heating capabilities of CNT doped nanocomposites by UV-Assisted Direct Write 3D printed technology were deeply explored to develop surface heating devices. First, a study of printability was carried out for different configurations regarding the location of the UV light guide during the printing process. This allows for optimizing the 3D printing manufacture of photocured resins doped with CNTs and analyzing the printing and curing steps, simultaneously or in consecutive steps. Then, the electrical conductivity and the Joule's heating capabilities were characterized as a function of the number of printed layers. The main goal of this work was the design and optimization of a low cost and easy to manufacture system, able to convert the surface of any structure into a heater with high efficiency for many future applications. Finally, a deicing test was carried out to prove the applicability of the printed circuits.

2. Materials and Methods

2.1. Materials

The 3D printing ink used was based on a commercial photocurable resin doped with CNTs. The matrix, HR Resin supplied by Iridium HiTech, was an acrylate-based resin

with a Shore hardness of 80D. On the other hand, CNTs were supplied by Nanocyl with the commercial name NC7000, which presented an average diameter of 9.5 nm and an average length of 1.5 μM . The substrate was a 2 mm thick fiberglass 0/90 woven fabric with the commercial name of Durostone EPC 203 and provided by Rochling with a gel-coat surface finish.

2.2. 3D Printing of Electrically Conductive Circuits

Prior to the 3D printing stage, nanocomposite conductive inks were prepared by a calendering dispersion process, based on a previously optimized 7-cycle method [35]. Here, the gap distance between rollers was reduced each cycle, keeping the speed of the rollers constant. Nanofiller content added was 0.5 wt.%. This CNT content, which was above the electrical percolation threshold, was high enough to ensure an efficient Joule's heating by applying a relatively low voltage. Moreover, this content was low enough to reduce, or even avoid, the UV shielding effect by CNTs, which hinders the photocuring reaction [24,36,37]. In this regard, an increase in the CNT content could cause a reduction in curing degree due to the increase in the UV-shielding effect, whereas a lower CNT content would induce a lower electrical conductivity of the nanocomposite and, therefore, a lower temperature reached by Joule's heating.

After the dispersion process, the mixture was 3D printed by UV-Assisted Direct Write technology, using a BCN3D Plus 3D printer by BCN3D Technologies with the Paste Extruder module, modified to allow the use of disposable syringes instead of the original container. Direct Write technique consists of extruding a viscous paste through a printing nozzle, depositing the material layer by layer until the 3D geometry is completed. Moreover, two different devices for adapting the UV lamp to the 3D printer were designed and tested. First, Figure 1a shows the 1-stage printing design, where the UV light guide was pointing directly to the extrusion nozzle. Here, the UV lamp was turned on during the material extrusion. In this regard, ink extrusion and curing took place in the same stage. On the other hand, Figure 1b shows the 2-stage printing design, where the UV light guide was not pointed directly to the extrusion nozzle. Here, the material was extruded in the first stage without UV irradiation and then, once the whole layer was extruded, a second stage was carried out where the UV light guide was placed perpendicularly to the printed circuit and irradiated the specimen, following the same path that the syringe did in the first stage. In this regard, ink extrusion and curing occurred in different stages. Both devices were 3D printed on PLA by Fused Filament Fabrication (FFF) with a BQ Witbox equipment supplied by BQ.

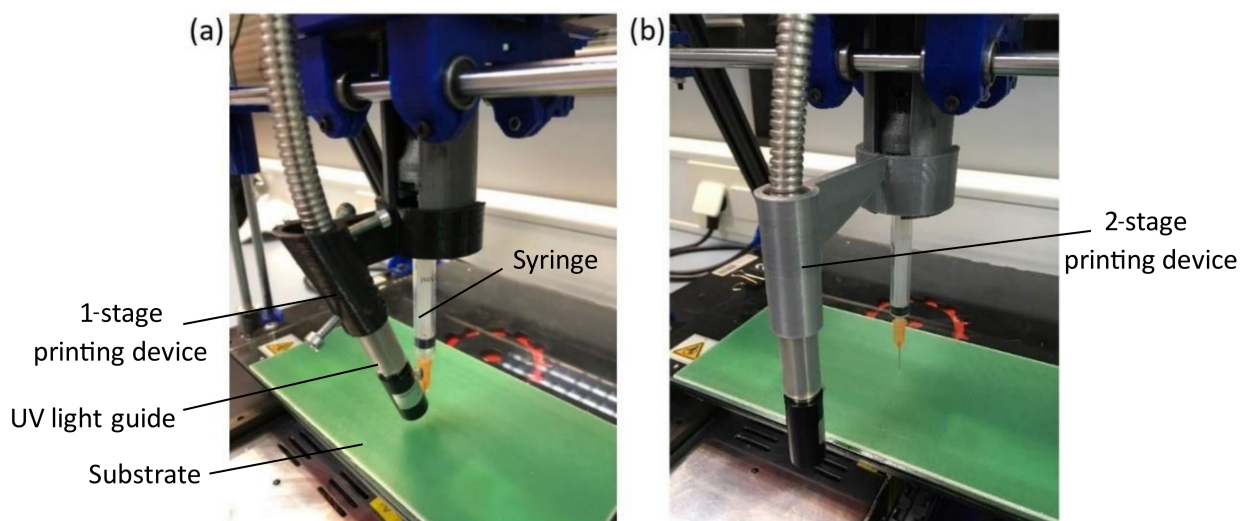


Figure 1. Alternative designs for housing the UV curing lamp to the 3D printer: (a) 1-stage printing device and (b) 2-stage printing device.

The UV lamp used was the LC8 model supplied by Hamamatsu, whose wavelength ranges from 240 to 400 nm. The UV lamp was equipped with the A10014-50-0110 light guide and the E5147-04 condenser lens, also supplied by Hamamatsu. The intensity was set to 100% and a distance between substrate and UV light of 10 mm was established since the maximum irradiance can be obtained with these parameters, allowing a faster curing of the printed ribbons during the 3D printing process.

The most relevant 3D printing parameters, defined with Slic3r software, are shown in Table 1.

Table 1. Experimental parameters of 3D printing.

Parameter	Value
Layer height (mm)	0.34
Number of skirt loops	2
Printing speed (mm/s)	7
Travel speed (mm/s)	25
Extrusion multiplier	0.6
Nozzle diameter (mm)	0.4
Retraction (mm)	0.5

The geometry of the printed specimens was based on a 4 parallel lines circuit (Figure 2) constituted by 1 to 4 printed layers. Each layer was printed as a single continuous line in order to avoid flow disruption in the 3D printer and, therefore, possible dimensional distortions in the printed circuits.

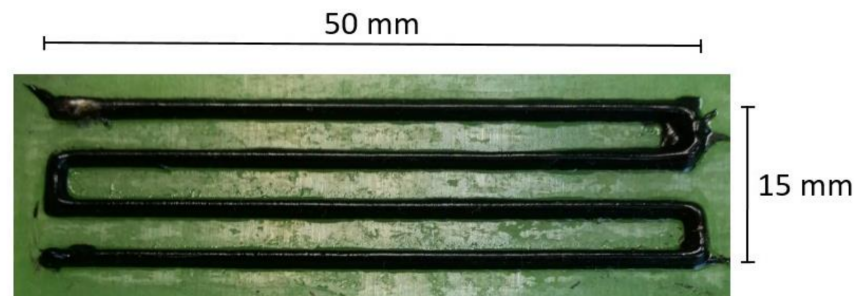


Figure 2. 3D printed circuit.

2.3. Characterization

2.3.1. Optimization of 3D-Printing Method

In order to compare the printability of the two alternative devices designed for housing the UV light guide (Figure 1), a morphological characterization was performed by image analysis with ImageJ software. The images were taken from the cross section of the printed ribbons with a Leica DMR Optical Microscope equipped with a Nikon 990 camera. The relevant parameters measured for the morphological characterization were the average height, width and cross-sectional area of the printed ribbons.

2.3.2. Electrical Conductivity

Electrical conductivity tests were carried out for the 3D printed circuits by obtaining the electrical resistance, R , from the V–I (Voltage–Intensity) slope using a voltage range from 0 to 50 V with a Keithley 2410 source-meter unit, supplied by Keithley Instruments. Then, the electrical conductivity was obtained based on the geometry of the specimens by the following expression (1), where L is distance between electrodes and A the cross-sectional area of the specimen.

$$\text{Electrical conductivity} = \frac{L}{A \cdot R} \quad (1)$$

The two main objectives of the electrical conductivity tests were to evaluate the electrical conductivity of the circuits as a function of the number of printed layers (1 to 4 layers) and, on the other hand, to study the influence of the interface between printed layers on the electrical conductivity. Regarding the last objective above mentioned, the electrical conductivity was measured for the ribbons with 2 to 4 layers by comparing two different electrode configurations, as shown in Figure 3. Figure 3a shows an electrode configuration within the same printed layer, while Figure 3b shows an electrode configuration with the electrodes placed in the first and the last printed layers, to evaluate the effect of the interface between printed layers on the electrical conductivity. A minimum of three measurements were carried out for each test in order to determine the mean value and the standard deviation between measurements.

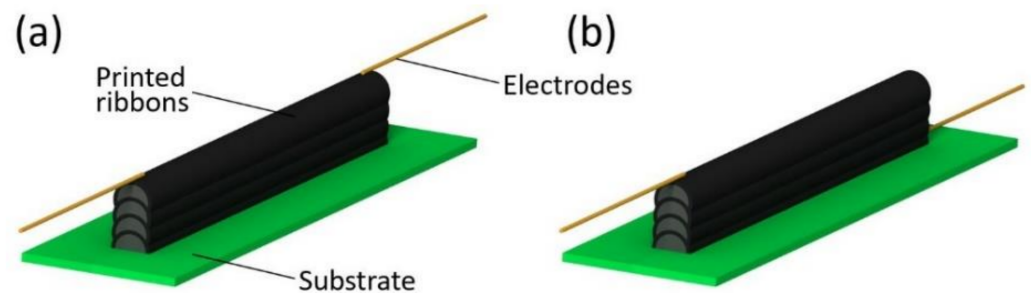


Figure 3. Scheme of electrode configuration for studying the effect of the interface between layers on the electrical conductivity of printed circuits. (a) electrodes placed in the same layer and (b) electrodes placed in the first and last printed layers.

2.3.3. Self-Heating by Joule's Effect

The self-heating capability of 3D printed circuits was characterized by Joule's heating tests, as shown in Figure 4a. Here, a power source (Keithley 2410 by Keithley Instruments) applied 200 V to the circuit with the 4 lines connected in parallel in order to heat the specimen by Joule's effect. In this regard, a thermal camera, FLIR E50 supplied by FLIR Instruments, measured the maximum and average temperature increments with regard to room temperature (ΔT_{\max} and ΔT_{av} , respectively). The region of thermal measurement was determined with FLIR Tools+ software, this being a rectangular area covering the whole circuit, as shown in Figure 4b. The Joule's heating tests were carried out in two different stages: first, the specimen was heated for 5 min by applying the above mentioned voltage with the power source and, then in the second stage the power source was turned off and the cooling of the specimen was also recorded for 5 min.

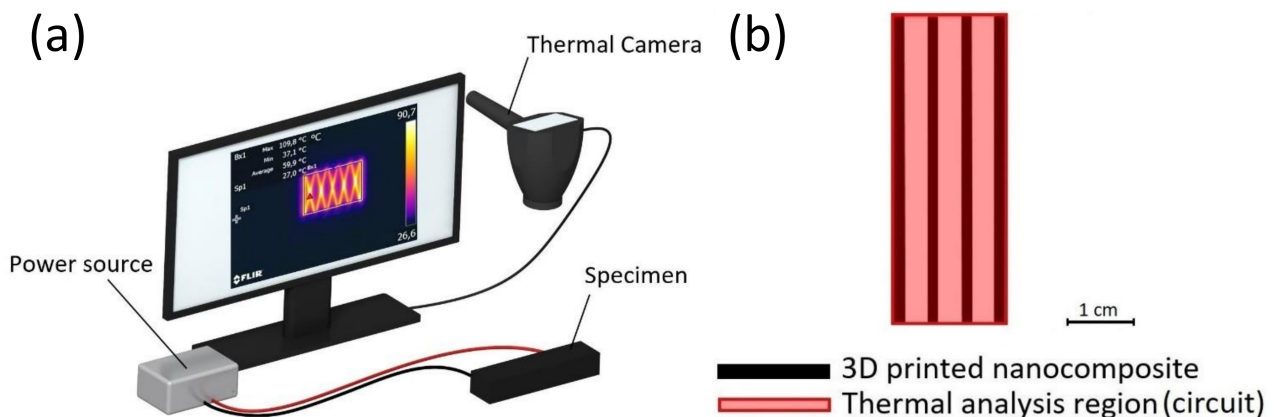


Figure 4. Self-heating tests. (a) Scheme of Joule's heating tests where a thermal camera is pointing to the specimen when heating by applying 200 V with the power source and (b) region of thermal analysis used with FLIR Tools+ software.

Moreover, a cycling test consisting of 5 heating and cooling cycles was carried out in order to demonstrate repeatability in self-heating. Furthermore, a heating test was carried out for 2 h to prove the stability of the system for long heating times.

2.3.4. Deicing Test

The deicing capability of the 4-layer circuit was tested. First, two circuits were coated with an approximately 2.5 mm thick ice layer by freezing deionized water at $-16\text{ }^{\circ}\text{C}$ for 2 h. Then, one of the circuits (heating circuit) was connected to the power source at 200 V, whereas the other circuit acted as a reference (reference circuit). The deicing time was measured by IR thermography by registering the temperature on specimen surface. A FLIR E50 thermal camera was pointing over the specimen surface placed in a vertical position to improve water removal.

3. Results and Discussion

3.1. Study of 3D Printing Quality

The results of the morphological characterization for comparing the two alternative designs for housing the UV light guide are shown in Figure 5.

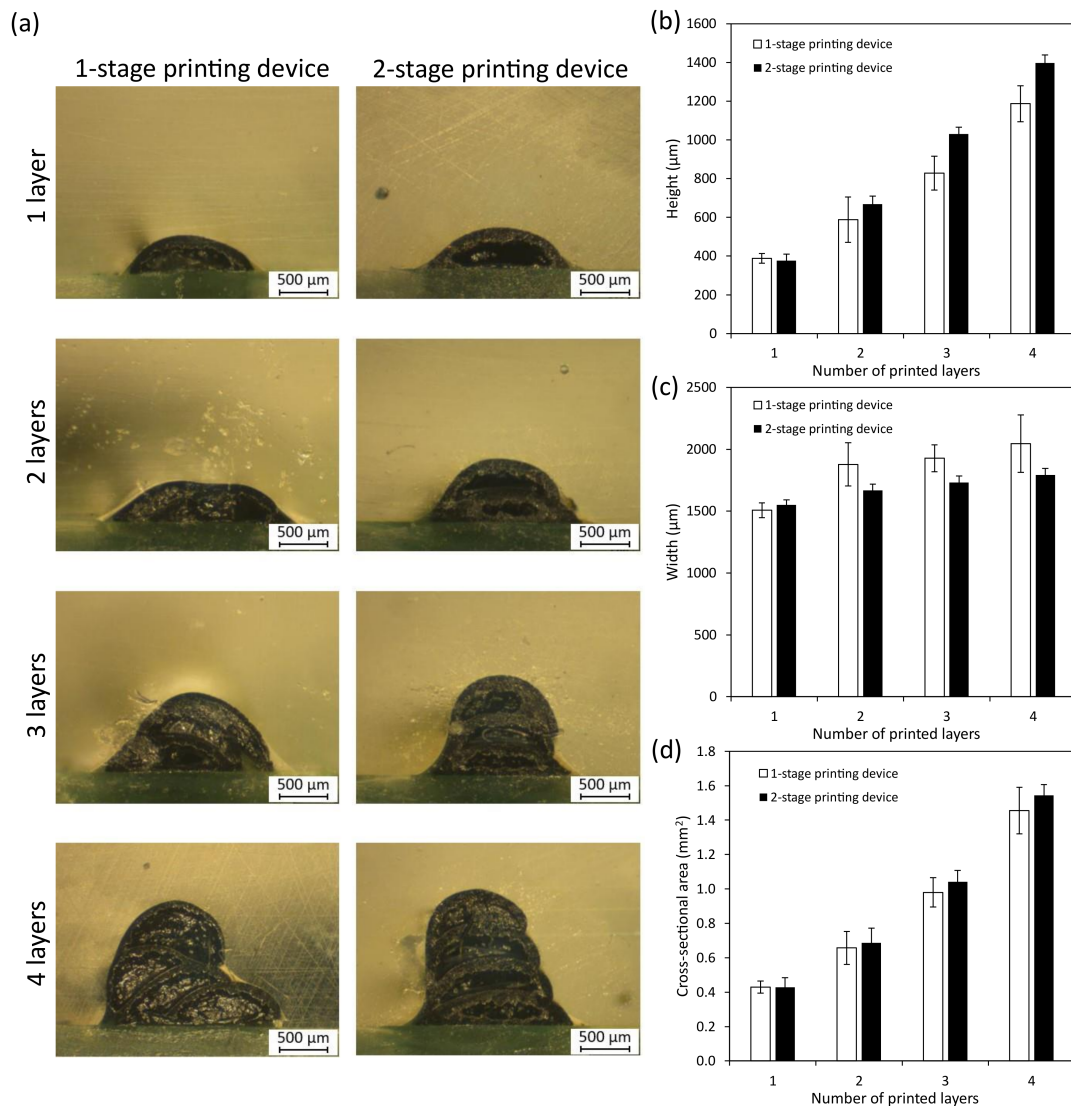


Figure 5. Morphological characterization as a function of the number of printed layers and the printed device used for housing the UV light guide. (a) Cross-section of the printed ribbons, (b) average height, (c) average width and (d) cross-sectional area.

First, Figure 5a shows the cross section of the 3D printed ribbons. Here, a significantly higher accuracy and a better distribution of the ribbons printed with the 2-stages printing device compared to the 1-stage printing device was observed when increasing the number of printed layers. In addition to this, the average height, width and cross-sectional area are analyzed in Figure 5b–d, respectively, as a function of the number of printed layers and the printed device used for housing the UV light guide. In this regard, the circuits printed with the 2-stage printing device showed a substantially higher height and a lower width compared to the circuits printed with the 1-stage printing device. The different quality of 3D printed circuits is explained by the different configuration and geometry of the device for housing the UV light guide used during the printing process. When using the 1-stage printing device, the UV light was pointing directly to the printing nozzle during the extrusion process. This may have totally or partially blocked the conductive ink flow due to the photopolymerization of the ink, which may have caused misalignment when extruding the ribbons. Moreover, the partial or total block of the printing nozzle due to the UV light can also cause substantial changes on the ink flow or even flow disruptions, which can be observed as a slight decrease in the cross-sectional area when using the 1-stage printing device. In this regard, the printability when using the 2-stages printing device was better, due to less misalignment that led to higher and narrower printed ribbons. Moreover, the cross-sectional area was not affected by partial or total clogs in the printing nozzle caused by UV light since the photopolymerization process occurred at a different stage than the extrusion process as the UV light was not pointed directly to the printing nozzle. Furthermore, the printing process was more robust and consistent, as the error bars of Figure 5b–d were wider for the 1-stage printing device as a result of higher differences between different measurements. For all these reasons above mentioned, it is highly recommended to select the 2-stage printing device for housing the UV light guide, in spite of the printing time, which is twice the printing time compared to using the 1-stage printing device.

3.2. Electrical Conductivity

Once the device for housing the UV light guide was selected due to the better distribution of the printed ribbons shown by the circuits made with the 2-stages printing device, electrical conductivity tests were performed (Figure 6).

First, Figure 6a shows the electrical conductivity of the circuits as a function of the number of printed layers. Here, the electrical conductivity values obtained for the specimens with different number of printed layers were in the same order of magnitude, in the range of 0.03–0.05 S/m, demonstrating the homogeneity of the printing ink and the reproducibility of the manufacturing process. However, when analyzing in detail, a slight increase in the electrical conductivity was observed when increasing the number of printed layers. Electrical conductivity is an intrinsic property of the material, so the value should not change when increasing the number of printed layers. However, the relatively small cross-sectional area of the printed ribbons makes them very sensitive to changes in the electrically conductive network formed by CNTs, which can be caused by presence of voids, changes in the ink flow through the printing nozzle, CNT aggregates or local heterogeneities, among others (Figure 6b). In this regard, the circuits which presented the highest cross-sectional area also presented the highest electrical conductivity due to the lower probability of containing critical defects that hindered the formation of the electrically conductive network. An ohmic behavior of the 3D printed nanocomposites was confirmed as there was a linear V-I correlation in the electrical test performed (see Figure S1).

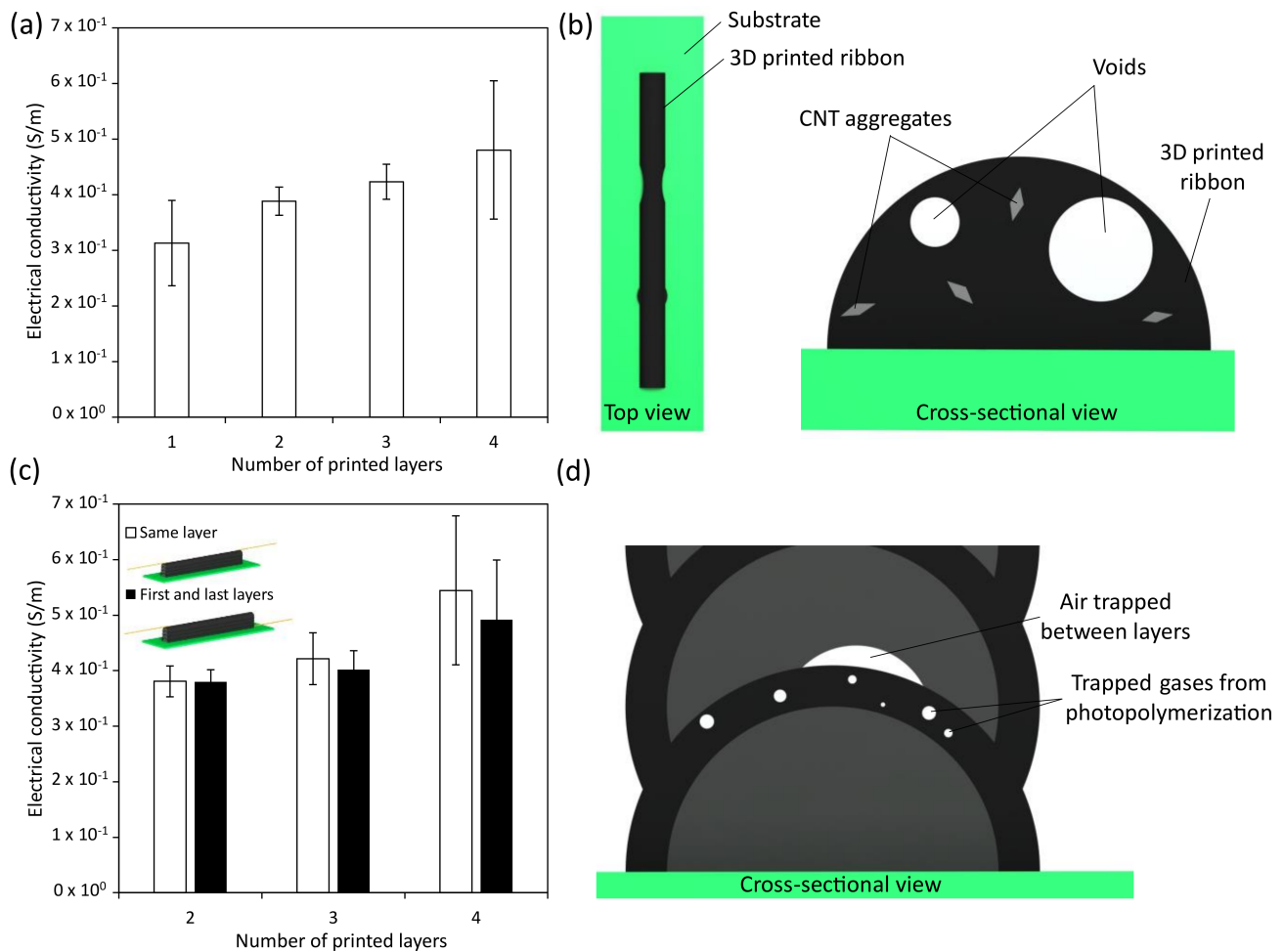


Figure 6. Electrical conductivity tests. (a) electrical conductivity of the circuits as a function of number of printed layers, (b) local heterogeneities that can hinder the formation of the electrically conductive network, (c) electrical conductivity of the ribbons as a function of electrode disposition and the number of printed layers and (d) scheme of air trapped between printed layers and trapped gases from the photocuring process.

Figure 6c shows the electrical conductivity of the ribbons as a function of the electrode configuration used for measuring (Figure 3), allowing us to study how the interface between layers affects the electrical conductivity. Here, a slight decrease in the electrical conductivity was observed for the tests carried out with the electrodes positioned in the first and last layers, which can be caused by some heterogeneities of trapped gases from the photopolymerization process or air trapped when depositing a new layer, as it is schematically shown in Figure 6d. Moreover, the decrease in the electrical conductivity observed in the specimens with the electrodes positioned in the first and last layers, with regard to the specimens with the electrodes positioned within the same layer, was higher when increasing the number of printed layers. These results support the statement above mentioned, regarding the negative effect of the printing defects when increasing the number of printing layers on the electrical conductivity. Furthermore, it has been proven that, despite the volumetric conductive network, the electrical current is able to flow through different pathways depending on the placement of the electrodes in the 3D printed circuits. Nevertheless, the electrical conductivity results evince that the interface between layers do not significantly affect the electrical conductivity of the circuits since the decrease in the electrical conductivity values was under 10% for the four-layer circuit.

Therefore, the electrical conductivity increased with the number of printed layers in spite of the evidence that there were structural defects at the interface between them.

Moreover, the electrical measurements have proven to be efficient and easy indirect tests to determine the quality of the printed circuits.

3.3. Self-Heating by Joule's Effect

Figure 7 shows the results of the self-heating test. First, Figure 7a shows ΔT_{max} and ΔT_{av} reached by Joule's heating of the 3D printed circuits as a function of the number of printed layers. Here, an increase in both the maximum and the average temperatures with the number of printed layers can be observed, which can be explained by the previously mentioned expression for the electrical conductivity (1). Here, the higher cross-sectional area (Figure 5d) and the higher electrical conductivity when increasing the number of printed layers (Figure 6a) are related to the lower electrical resistance of the printed circuits. Furthermore, according to Ohm's law (2), a decrease in the electrical resistance is related to an increase in the intensity, I , for the same applied voltage, V , and, according to Joule's heating law (3), the heat generated during Joule's heating test, Q , is related to the square of the intensity.

$$V = I \cdot R \tag{2}$$

$$Q = I^2 \cdot R \cdot t \tag{3}$$

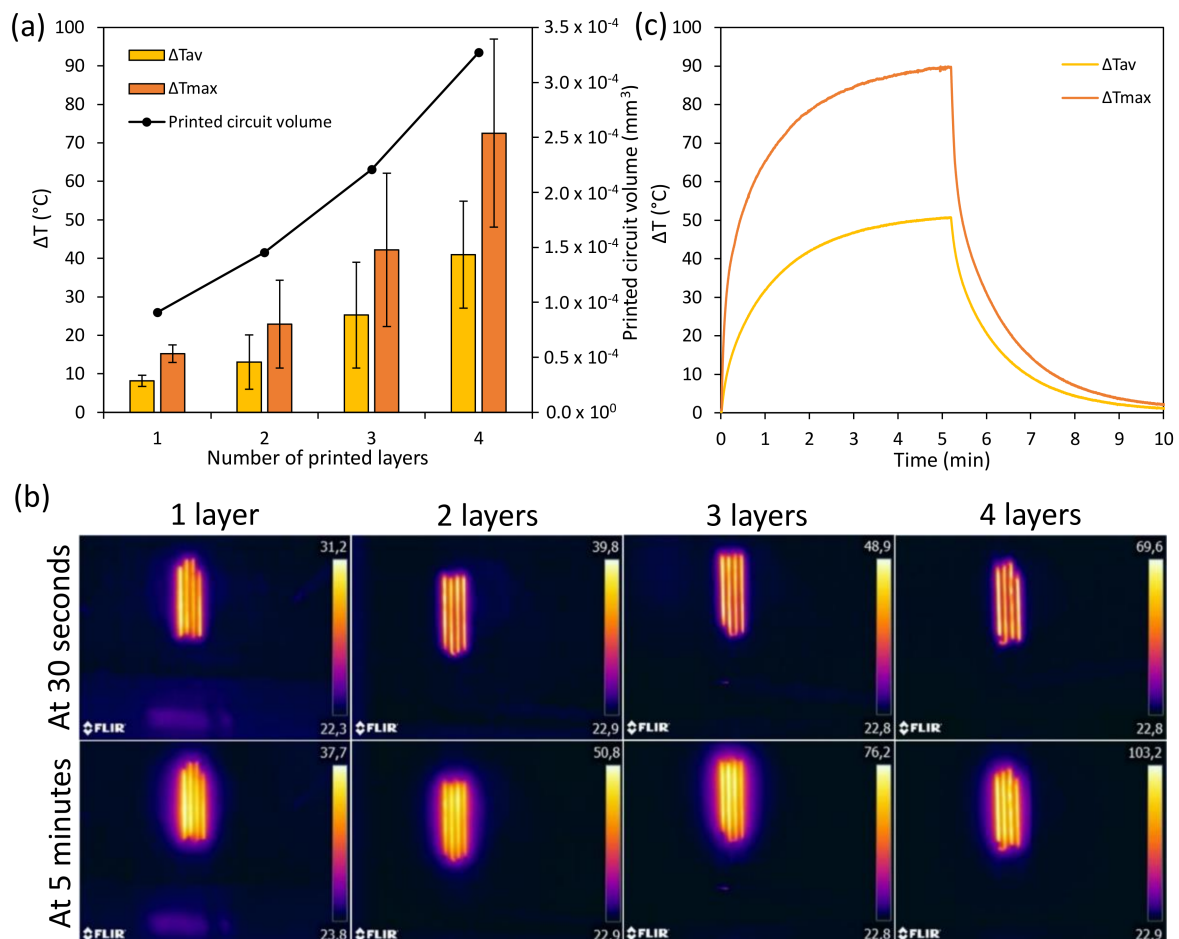


Figure 7. Self-heating tests by Joule's heating. (a) Average and maximum temperature increment with respect to room temperature (left axis), and printed circuit volume (right axis) as a function of the number of printed layers, (b) IR images at different heating times during self-heating tests as a function of the number of printed layers and (c) self-heating test of a 4-layer circuit showing average and maximum temperature increments of the circuit as a function of time.

In this regard, the higher amount of printed material the circuit presents, the higher temperature it reaches by Joule's heating. Furthermore, by increasing the number of layers,

the specific area of the printed circuit decreases (Figure 5d), thus minimizing heat losses. On the other hand, the difference observed between ΔT_{\max} and ΔT_{av} values is explained because of the non-heated substrate. The standard deviation between different measurements can be caused by homogeneity issues in the printed circuits. Nevertheless, the self-heating tests showed great results in terms of heating capability with the relatively low applied voltage in comparison with previous studies performed with thermally cured resins and much higher carbon nanoparticle contents [24,38]. In this context, the four-layer circuit would be suitable for deicing purposes even in $-30\text{ }^{\circ}\text{C}$ conditions since it is capable of reaching an average temperature increment with respect to room temperature above $30\text{ }^{\circ}\text{C}$ [39].

On the other hand, the IR images shown in Figure 7b demonstrate the fast and homogeneous heating achieved by the printed circuits. Here, the slight temperature differences along the circuit can be caused by local heterogeneities of the nanocomposite, such as CNT aggregates, that could lead to the presence of high and low electrically conductive areas.

Moreover, Figure 7c shows an example of the ΔT_{\max} and ΔT_{av} as a function of time during a self-heating test carried out for a four-layer circuit. Here, the fast heating of the circuit can be noticed since it was able to reach a temperature increment with regard to room temperature of around $30\text{ }^{\circ}\text{C}$ within 1 min.

Figure 8a shows a cyclic self-heating test. Here, a great repeatability in the temperature reached by Joule's heating can be observed among the five cycles of heating and cooling, since the deviation in the temperature reached was below 3%. Moreover, the self-heating test carried out for 2 h of continuous heating (Figure 8b) showed an ever-increasing temperature with time due to the ever-higher electron mobility promoted by the temperature increase. In addition, it has been proven that the temperature homogeneity in the printed circuits does not vary (see the IR images taken at 15 and 120 min), proving their excellent performance when heating for long periods of time.

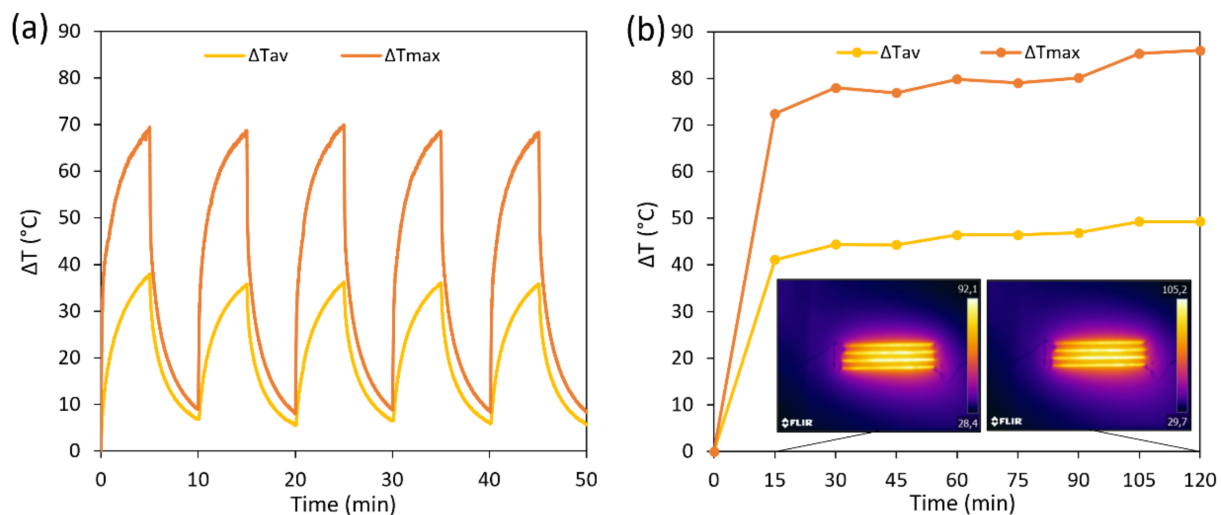


Figure 8. (a) Cyclic self-heating test and (b) continuous self-heating test carried out for 2 h.

In summary, 3D printing of nanodoped circuits has emerged as an easy procedure to convert any structure in an efficient surface heater with low power consumption.

Figure 9 shows the deicing test carried out for the four-layer circuit. Here, it can be observed that the heating circuit (right), which was connected to the power source at 200 V, was able to remove an approximately 2.5 mm thick ice layer in 4 min and 4 s, whereas the ice layer on the reference circuit (left) remained almost unaltered. The deicing time was set as the time when the ice layer slides off the circuit (see IR images), correlated to the increase in the temperature of the circuit's area above $0\text{ }^{\circ}\text{C}$.

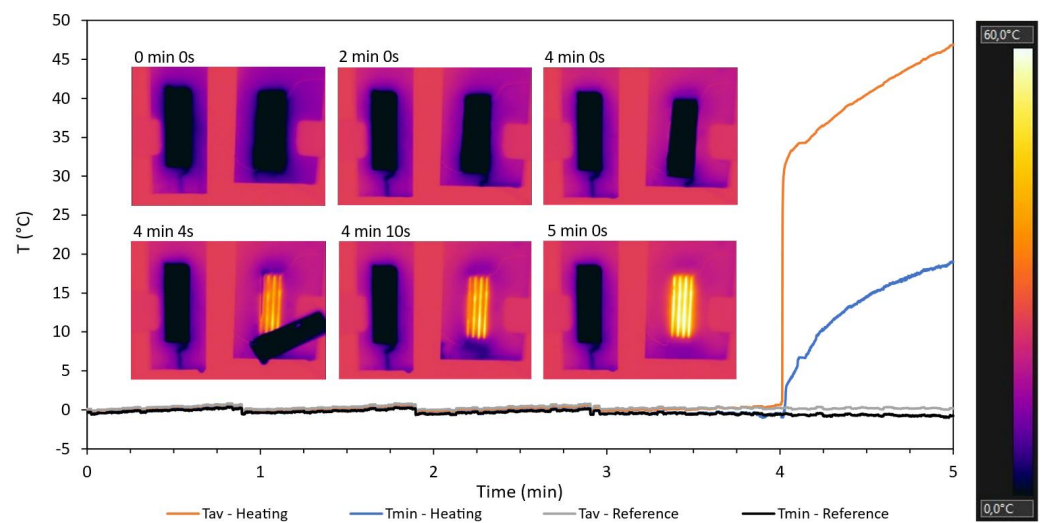


Figure 9. Deicing test with IR images taken at different times.

4. Conclusions

The electrical and electrothermal capabilities of 3D printed circuits by UV-Assisted Direct Write technology have been extensively studied as a function of the number of printed layers. First, an analysis of printability by comparing two alternative designs for housing the UV light guide was carried out. Here, the two-stage printing device, which allows curing of the circuit in a separate stage to the material extrusion, showed a significantly higher printability and reproducibility compared to the one-stage printing device since the printed ribbons showed a higher height and a lower width. In this regard, the one-stage printing device, which simultaneously extrudes and cures the ink, may cause a total or partial block of the conductive ink flow due to the photopolymerization of the ink inside the syringe, leading to misalignment and a reduction in the ink flow when extruding the ribbons.

On the other hand, electrical conductivity tests showed a slight increase in electrical conductivity with the number of printed layers. Despite the electrical conductivity, which is an intrinsic property of the material, the relatively small cross-sectional area of the printed ribbons makes them very sensitive to changes in the electrically conductive network formed by CNTs as the presence of voids or CNT aggregates. In this regard, the higher the cross-sectional area, the lower probability of finding a critical defect that hinders the formation of the electrically conductive network. In addition, the interface between layers slightly reduced the electrical conductivity of the printed ribbons due to printing defects caused by gas trapped during photopolymerization or air trapped when extruding an additional layer.

The self-heating tests showed a significant increase in the temperature reached by Joule's effect with the number of printed layers due to the decrease in the electrical resistance when increasing the cross-sectional area. This led to a higher electrical intensity and thus to a higher heat generated during Joule's heating test. Furthermore, the great homogeneity and repeatability of the heating showed by the printed circuits, together with their excellent performance for long heating times, proved their applicability to convert any structure in an efficient surface heater with low power consumption.

Finally, the deicing capability of the four-layer circuit was demonstrated, being able to remove a 2.5 mm thick ice layer in 4 min and 4 s.

Supplementary Materials: The following are available online at <https://www.mdpi.com/article/10.3390/app11167534/s1>.

Author Contributions: Conceptualization, A.C., M.C., A.J.-S.; methodology, A.C.; formal analysis, A.C.; data curation, A.C.; writing—original draft preparation, A.C.; writing—review and editing,

A.J.-S., M.C., A.U., S.G.P.; funding acquisition A.J.-S., M.C., A.U. and S.G.P. All authors have read and agreed to the published version of the manuscript.

Funding: This work was supported by the Ministerio de Economía y Competitividad of Spain Government [PID2019-106703RB-I00]; Comunidad de Madrid Government [ADITIMAT-CM S2018/NMT-4411] and Young Researchers R&D Project (Ref. M2183, SMART-MULTICOAT) financed by Universidad Rey Juan Carlos and Comunidad de Madrid.

Data Availability Statement: The data presented in this study are available on request from the corresponding author.

Conflicts of Interest: The authors declare no conflict of interest.

References

1. Thomas, D.S.; Gilbert, S.W. *Costs and Cost Effectiveness of Additive Manufacturing*; NIST Special Publication 1176; NIST: Gaithersburg, MD, USA, 2014.
2. Singh, R.; Singh, S.; Nanak, G.; Engineering, D. Additive Manufacturing: An Overview. In *Reference Module in Materials Science and Materials Engineering*; Elsevier Ltd.: Amsterdam, Netherlands, 2017; pp. 1–12. ISBN 9780128035818.
3. Conner, B.P.; Manogharan, G.P.; Martof, A.N.; Rodomsky, L.M.; Rodomsky, C.M.; Jordan, D.C.; Limperos, J.W. Making sense of 3-D printing: Creating a map of additive manufacturing products and services. *Addit. Manuf.* **2014**, *1–4*, 64–76. [[CrossRef](#)]
4. Mehrpouya, M.; Dehghanghadikolaie, A.; Fotovvati, B.; Vosooghnia, A.; Emamian, S.S.; Gisario, A. The potential of additive manufacturing in the smart factory industrial 4.0: A review. *Appl. Sci.* **2019**, *9*, 3865. [[CrossRef](#)]
5. Alogla, A.A.; Baumers, M.; Tuck, C.; Elmadih, W. The Impact of Additive Manufacturing on the Flexibility of a Manufacturing Supply Chain. *Appl. Sci.* **2021**, *11*, 3707. [[CrossRef](#)]
6. Zhang, Y.; Xu, Y.; Simon-Masseron, A.; Lalevé, J. Radical photoinitiation with LEDs and applications in the 3D printing of composites. *Chem. Soc. Rev.* **2021**, *50*, 3824–3841. [[CrossRef](#)] [[PubMed](#)]
7. Bourell, D.; Kruth, J.P.; Leu, M.; Levy, G.; Rosen, D.; Beese, A.M.; Clare, A. Materials for additive manufacturing. *CIRP Ann. Manuf. Technol.* **2017**, *66*, 659–681. [[CrossRef](#)]
8. Zhang, Y.; Josien, L.; Salomon, J.-P.; Simon-Masseron, A.; Lalevé, J. Photopolymerization of Zeolite/Polymer-Based Composites: Toward 3D and 4D Printing Applications. *Cite ACS Appl. Polym. Mater.* **2020**, *2021*, 400–409. [[CrossRef](#)]
9. Pezzana, L.; Riccucci, G.; Spriano, S.; Battezzore, D.; Sangermano, M.; Chiappone, A. 3D Printing of PDMS-Like Polymer Nanocomposites with Enhanced Thermal Conductivity: Boron Nitride Based Photocuring System. *Nanomaterials* **2021**, *11*, 373. [[CrossRef](#)] [[PubMed](#)]
10. Chou, P.-Y.; Chou, Y.-C.; Lai, Y.-H.; Lin, Y.-T.; Lu, C.-J.; Liu, S.-J.; Chou, P.-Y.; Chou, Y.-C.; Lai, Y.-H.; Lin, Y.-T.; et al. Fabrication of Drug-Eluting Nano-Hydroxylapatite Filled Polycaprolactone Nanocomposites Using Solution-Extrusion 3D Printing Technique. *Polymers* **2021**, *13*, 318. [[CrossRef](#)] [[PubMed](#)]
11. Ngo, T.D.; Kashani, A.; Imbalzano, G.; Nguyen, K.T.Q.; Hui, D. Additive manufacturing (3D printing): A review of materials, methods, applications and challenges. *Compos. Part B* **2018**, *143*, 172–196. [[CrossRef](#)]
12. Wang, X.; Jiang, M.; Zhou, Z.; Gou, J.; Hui, D. 3D printing of polymer matrix composites: A review and prospective. *Compos. Part B* **2017**, *110*, 442–458. [[CrossRef](#)]
13. Ligon, S.C.; Liska, R.; Stampfl, J.; Gurr, M.; Mühlaupt, R. Polymers for 3D Printing and Customized Additive Manufacturing. *Chem. Rev.* **2017**, *117*, 10212–10290. [[CrossRef](#)] [[PubMed](#)]
14. Valentine, A.D.; Busbee, T.A.; Boley, J.W.; Raney, J.R.; Chortos, A.; Kotikian, A.; Berrigan, J.D.; Durstock, M.F.; Lewis, J.A. Hybrid 3D Printing of Soft Electronics. *Adv. Mater.* **2017**, *29*, 1703817. [[CrossRef](#)]
15. Adib, A.A.; Sheikhi, A.; Shahhosseini, M.; Simeunović, A.; Wu, S.; Castro, C.E.; Zhao, R.; Khademhosseini, A.; Hoelzle, D.J. Direct-write 3D printing and characterization of a GelMA-based biomaterial for intracorporeal tissue engineering. *Biofabrication* **2020**, *12*, 045006. [[CrossRef](#)] [[PubMed](#)]
16. Yang, F.; Zhang, M.; Bhandari, B.; Liu, Y. Investigation on lemon juice gel as food material for 3D printing and optimization of printing parameters. *LWT Food Sci. Technol.* **2018**, *87*, 67–76. [[CrossRef](#)]
17. Farahani, R.D.; Daniel, T.; Dubé, M.; Bodkhe, S.; Mahdavi, M. Additive Manufacturing of Multifunctional Nanocomposites and Composites. In *Reference Module in Materials Science and Materials Engineering*; Elsevier Ltd.: Amsterdam, The Netherlands, 2018; Volume 6, pp. 380–407. ISBN 9780128035818.
18. Shen, A.; Bailey, C.P.; Ma, A.W.K.; Dardona, S. UV-assisted direct write of polymer-bonded magnets. *J. Magn. Magn. Mater.* **2018**, *462*, 220–225. [[CrossRef](#)]
19. Thakur, A.; Dong, X. Printing with 3D continuous carbon fiber multifunctional composites via UV-assisted coextrusion deposition. *Manuf. Lett.* **2020**, *24*, 1–5. [[CrossRef](#)]
20. Wei, H.; Zhang, Q.; Yao, Y.; Liu, L.; Liu, Y.; Leng, J. Direct-write fabrication of 4D active shape-changing structures based on a shape memory polymer and its nanocomposite. *ACS Appl. Mater. Interfaces* **2017**, *9*, 876–883. [[CrossRef](#)]
21. Podsiadły, B.; Matuszewski, P.; Skalski, A.; Słoma, M. Carbon Nanotube-Based Composite Filaments for 3D Printing of Structural and Conductive Elements. *Appl. Sci.* **2021**, *11*, 1272. [[CrossRef](#)]

22. Kim, G.; Vu, C.C.; Kim, J. Single-layer pressure textile sensors withwoven conductive yarn circuit. *Appl. Sci.* **2020**, *10*, 2877. [[CrossRef](#)]
23. Rathinavel, S.; Priyadarshini, K.; Panda, D. A review on carbon nanotube: An overview of synthesis, properties, functionalization, characterization, and the application. *Mater. Sci. Eng. B* **2021**, *268*, 115095. [[CrossRef](#)]
24. Cortés, A.; Jiménez-Suárez, A.; Campo, M.; Ureña, A.; Prolongo, S.G. 3D printed epoxy-CNTs/GNPs conductive inks with application in anti-icing and deicing systems. *Eur. Polym. J.* **2020**, *141*, 110090. [[CrossRef](#)]
25. Hwan Kwon, O.; Kim, J.; Koh, W.G.; Kang, Y.H.; Jang, K.S.; Cho, S.Y.; Yoo, Y. Flexible and free-standing thermoelectric devices prepared from poly(vinylidene fluoride-co-hexafluoropropylene)/graphite nanoplatelet/single-walled carbon nanotube composite films. *Mater. Sci. Eng. B* **2019**, *243*, 199–205. [[CrossRef](#)]
26. Luo, Y.; Wu, D.; Zhao, Y.; Chen, Q.; Xie, Y.; Wang, M.; Lin, L.; Wang, L.; Sun, D. Direct write of a flexible high-sensitivity pressure sensor with fast response for electronic skins. *Org. Electron.* **2019**, *67*, 10–18. [[CrossRef](#)]
27. Farahani, R.D.; Dalir, H.; Le Borgne, V.; Gautier, L.A.; El Khakani, M.A.; Lévesque, M.; Therriault, D. Direct-write fabrication of freestanding nanocomposite strain sensors. *Nanotechnology* **2012**, *23*, 085502. [[CrossRef](#)] [[PubMed](#)]
28. Aissa, B.; Therriault, D.; Farahani, D.; Lebel, L.; El Khakani, A.; Assa, B.; Therriault, D.; Farahani, R.D.; Lebel, L.L.; El Khakani, M.A. Electrical transport properties of single wall carbon nanotube/polyurethane composite based field effect transistors fabricated by UV-assisted direct-writing technology. *Nanotechnology* **2012**, *23*, 115705. [[CrossRef](#)]
29. Parent, O.; Ilinca, A. Anti-icing and deicing techniques for wind turbines: Critical review. *Cold Reg. Sci. Technol.* **2011**, *65*, 88–96. [[CrossRef](#)]
30. Christ, J.F.; Aliheidari, N.; Pötschke, P.; Ameli, A. Bidirectional and stretchable piezoresistive sensors enabled by multimaterial 3D printing of carbon nanotube/thermoplastic polyurethane nanocomposites. *Polymers* **2018**, *11*, 11. [[CrossRef](#)] [[PubMed](#)]
31. Ilanchezhian, P.; Zakirov, A.S.; Kumar, G.M.; Yuldashev, S.U.; Cho, H.D.; Kang, T.W.; Mamadalimov, A.T. Highly efficient CNT functionalized cotton fabrics for flexible/wearable heating applications. *RSC Adv.* **2015**, *5*, 10697–10702. [[CrossRef](#)]
32. Kim, H.S.; Ban, H.; Park, W.J. Deicing concrete pavements and roads with Carbon Nanotubes (CNTs) as heating elements. *Materials* **2020**, *13*, 2504. [[CrossRef](#)]
33. Gohardani, O.; Elola, M.C.; Elizetxea, C. Potential and prospective implementation of carbon nanotubes on next generation aircraft and space vehicles: A review of current and expected applications in aerospace sciences. *Prog. Aerosp. Sci.* **2014**, *70*, 42–68. [[CrossRef](#)]
34. Tarfaoui, M.; El Moumen, A.; Boehle, M.; Shah, O.; Lafdi, K. Self-heating and deicing epoxy/glass fiber based carbon nanotubes buckypaper composite. *J. Mater. Sci.* **2019**, *54*, 1351–1362. [[CrossRef](#)]
35. Jiménez-Suárez, A.; Campo, M.; Sánchez, M.; Romón, C.; Ureña, A. Dispersion of carbon nanofibres in a low viscosity resin by calendering process to manufacture multiscale composites by VARIM. *Compos. Part B Eng.* **2012**, *43*, 3104–3113. [[CrossRef](#)]
36. Cortés, A.; Sánchez-Romate, X.F.; Jiménez-Suárez, A.; Campo, M.; Ureña, A.; Prolongo, S.G. Mechanical and strain-sensing capabilities of carbon nanotube reinforced composites by digital light processing 3D printing technology. *Polymers* **2020**, *12*, 975. [[CrossRef](#)] [[PubMed](#)]
37. Cortés, A.; Sánchez-Romate, X.F.; Jiménez-Suárez, A.; Campo, M.; Esmaeili, A.; Sbarufatti, C.; Ureña, A.; Prolongo, S.G. Complex Geometry Strain Sensors Based on 3D Printed Nanocomposites: Spring, Three-Column Device and Footstep-Sensing Platform. *Nanomaterials* **2021**, *11*, 1106. [[CrossRef](#)]
38. Cortés, A.; Sánchez-Romate, X.F.; Jiménez-Suárez, A.; Campo, M.; Prolongo, M.G.; Ureña, A.; G Prolongo, S. 3D printed anti-icing and deicing system based on CNT/GNP doped epoxy composites with self-curing and structural health monitoring capabilities. *Smart Mater. Struct.* **2021**, *30*, 025016. [[CrossRef](#)]
39. Redondo, O.; Prolongo, S.G.; Campo, M.; Sbarufatti, C.; Giglio, M. Anti-icing and deicing coatings based Joule's heating of graphene nanoplatelets. *Compos. Sci. Technol.* **2018**, *164*, 65–73. [[CrossRef](#)]